Noncontact modulated laser calorimetry of liquid silicon in a static magnetic field

Noncontact modulated laser calorimetry of liquid silicon in a static magnetic field

Hidekazu Kobatake,[1,a)] Hiroyuki Fukuyama,[1] Izuru Minato,[1] Takao Tsukada,[2] and Satoshi Awaji[3]

[1]*Institute of Multidisciplinary Research for Advanced Materials, Tohoku University, 2-1-1 Katahira, Aoba-ku, Sendai 980-8577, Japan*
[2]*Department of Chemical Engineering, Osaka Prefecture University, 1-1 Gakuen-cho, Sakai, Osaka 599-8531, Japan*
[3]*Institute for Materials Research, Tohoku University, 2-1-1 Katahira, Aoba-ku, Sendai 980-8577, Japan*

Accurate thermal transport properties of high-temperature liquid silicon, such as those of heat capacity, emissivity, and thermal conductivity, are required for improving numerical modeling to produce high-quality silicon crystals using the Czochralski method. However, contamination from contact material and convection complicates measurements of these properties. The authors developed a noncontact modulated laser calorimetry using electromagnetic levitation in a static magnetic field. The isobaric molar heat capacity, thermal conductivity, and hemispherical total emissivity of liquid silicon were measured simultaneously at temperatures of 1750–2050 K. Convection in the levitated liquid silicon was suppressed above a static magnetic field of 2 T. © *2008 American Institute of Physics.* [DOI: 10.1063/1.2966455]

I. INTRODUCTION

To maintain global competitiveness in the silicon wafer industry, demand is a growing for large, high-quality silicon crystals. Bulk silicon crystal is currently produced with a 12 in. diameter using the Czochralski method. Furthermore, production of 16 in. diameter crystals is anticipated in the near future. To realize such a large crystal, heat transport across the solid/liquid interface of silicon must be well understood by numerical modeling. For that modeling, accurate knowledge of liquid silicon's thermophysical properties, such as heat capacity, thermal conductivity, and emissivity, is indispensable.[1] However, these properties, which are used in numerical modeling, present a wide variation.[2] The salient difficulties of the measurement of thermal conductivity are posed by natural and Marangoni convections. Chemical reactions between molten silicon and contact materials also increase the experimental uncertainty.

Fecht and co-workers[3–6] developed ac calorimetry for an electromagnetically levitated high-temperature metallic liquid using a radio-frequency (rf) coil. The modulated power of the rf coil sinusoidally heats the samples. Using such a coil, they measured the heat capacity and emissivity without contamination. In theory, the thermal conductivity can be measured by analyzing the phase shift between the modulation heating and temperature response. However, the thermal conductivity measured using this technique is affected by convection in the melt. Yasuda *et al.*[7] reported that surface oscillations and convection in the electromagnetically levitated liquid metal were suppressed by the Lorenz force in a static magnetic field.

Based on the technique described above,[3–7] we have developed a noncontact modulated laser calorimetry technique for the electromagnetically levitated high-temperature liquid in a static magnetic field with suppression of convection. Tsukada *et al.*[8] described the theory and validity of this technique using numerical simulation. In addition, the experimental principle was verified using a solid platinum sphere as a reference.[9] Results of thermal conductivity of liquid silicon were separately reported;[10] they show that the electron contribution is dominant for thermal transport in liquid silicon. This report describes more details related to the noncontact calorimetry of liquid silicon. Results of the heat capacity and hemispherical total emissivity are presented with those for thermal conductivity.

II. PRINCIPLE OF MODULATED LASER CALORIMETRY

A. Heat capacity

Details of the experimental principle are explained by Fukuyama *et al.*[9] Here, a brief outline is described. Figures 1(a) and 1(b), respectively, portray schematic illustrations of the experimental apparatus and a heat flow model of noncontact modulated laser calorimetry. The top surface of the silicon droplet, levitated in vacuum, is heated with angular frequency ω (rad s^{-1}) using a modulated laser with a form of $p_o(1+\cos \omega t)$ (W m^{-2}). The temperature response at the bottom surface of the droplet is measured using a pyrometer. The heat balances in this system are as follows.

The heat balance at laser-irradiated part is

$$V_h C_p \frac{dT_h}{dt} = Q_h + \alpha S_h A p_o (1 + \cos \omega t) - S_h A \varepsilon \sigma (T_h^4 - T_\infty^4)$$

$$- K_c (T_h - T)_l, \tag{1}$$

that at the laser-nonirradiated part is

a)Author to whom correspondence should be addressed. Electronic mail: kobatake@tagen.tohoku.ac.jp.
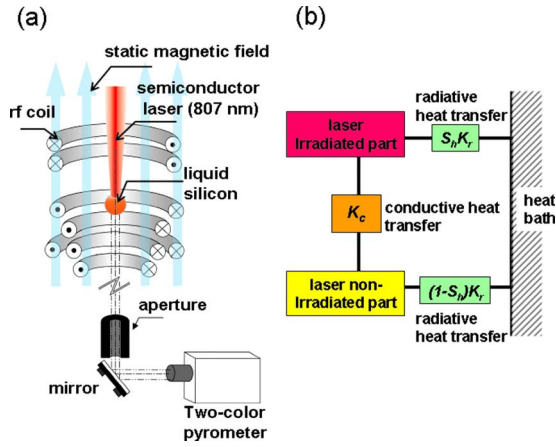
(a)

FIG. 1. (Color online) (a) Schematic illustration of the electromagnetic levitation apparatus and (b) heat flow model for this noncontact modulated laser calorimetry.

$$(1 - V_h)C_p \frac{dT_l}{dt} = Q_l + (1 - S_h)A\varepsilon\sigma(T_l^4 - T_\infty^4) + K_c(T_h - T)_l. \tag{2}$$

In those equations, S_h is the fraction of the irradiated surface area that is heated by the laser, V_h denotes the volume fraction corresponding to S_h, C_p (J K^{-1}) represents the isobaric heat capacity, T (K) is the absolute temperature, Q (W) is the power input from the rf coil, α is the absorptivity, A (m^2) is the surface area of the droplet, K_c (W K^{-1}) is the thermal conductance for conductive heat transfer from the laser-irradiated part to the nonirradiated part, K_r (W K^{-1}) is the thermal conductance for radiative heat transfer from the sample surface to the heat reservoir in vacuum, ε is the hemispherical total emissivity, and σ(W m^{-2} K^{-4}) is the Stefan–Boltzmann constant. Subscripts h and l, respectively, denote the laser-irradiated part and nonirradiated part. The sample temperature is expressed as the sum of the initial temperature T_0, the average increase in temperature ΔT_{dc} (dc component), and the modulation amplitude $\Delta T_{ac} \cos(\omega t - \phi)$ (ac component) as

$$T = T_0 + \Delta T_{dc} + \Delta T_{ac} \cos(\omega t - \varphi). \tag{3}$$

By solving Eqs. (1) and (2) under the condition of $K_r/K_c \leq 1$, where $K_r = 4A\varepsilon\sigma T_0^3$, the phase shift ϕ between the laser signal and temperature response and the temperature amplitude ΔT_{ac} are expressed as follows:[9]

$$\Delta T_{ac} = \frac{\alpha S_h A p_0}{\omega C_p}\left\{1 + \frac{1}{\omega^2\tau_r^2} + \omega^2\tau_c^2\right\}^{-1/2}, \tag{4}$$

$$\cos\varphi = \frac{\tau_c}{\omega}\left\{\frac{1}{\tau_c\tau_r} - \omega^2\right\}\left\{1 + \frac{1}{\omega^2\tau_r^2} + \omega^2\tau_c^2\right\}^{-1/2}. \tag{5}$$

Therein, τ_r (s) is the external thermal relaxation time attributable to the radiative heat transfer and τ_c (s) is the internal thermal relaxation time attributable to the conductive heat transfer in the silicon. These relaxation times are defined as

$$\tau_r = \frac{C_p}{K_r} = \frac{C_p}{4A\varepsilon\sigma T_0^3} \tag{6}$$

and

$$\tau_c = \frac{C_p}{K_c} = V_h(1 - V_h), \tag{7}$$

where σ is the Stefan–Boltzmann constant. The term $\alpha S_h A p_0$ in Eq. (4) is evaluated quantitatively using the products of the laser power and the normal spectral emissivity at a laser wavelength of the object. Assuming Kirchhoff's law, the normal spectral emissivity is used as the absorptivity. For this study, the value of the normal spectral emissivity of liquid silicon ε_s is 0.223 at the laser wavelength (807 nm) measured at 1553–1797 K with an uncertainty of 5%.[11] The distribution of the laser intensity is Gaussian; the e^{-2} radius of the laser beam is 2 mm for a liquid silicon droplet of 4 mm radius. Effects of the sample curvature on the absorptivity were ignored.

The correction function f is defined as

$$f = \left\{1 + \frac{1}{\omega^2\tau_r^2} + \omega^2\tau_c^2\right\}^{-1/2}. \tag{8}$$

The condition $\omega^2\tau_r^2 \gg 1 \gg \omega^2\tau_c^2$, which satisfies $f \cong 1$, is achieved by a proper choice of the modulation frequency. The heat capacity is therefore determined by the temperature amplitude from Eq. (4). Under this condition, the correction function f has a maximum value, close to unity, against the modulation frequency, i.e., the function $\omega\Delta T_{ac}$ has a maximum value as a function of the modulation frequency. At that modulation frequency, the phase difference is equal to 90°, as derived from the requirement of $\partial f/\partial\omega = 0$. Therefore, the heat capacity is determined experimentally from the temperature amplitude, satisfying the above requirement.

Equation (5) shows that the phase shift at a lower modulation frequency is strongly dependent on the external thermal relaxation time; the phase shift at higher frequency is controlled by the internal thermal relaxation time. However, this simple treatment described above is insufficient to determine both thermal conductivity and emissivity of the liquid silicon. It is necessary to analyze the heat flow in the droplet more accurately to determine both thermal conductivity and emissivity from the phase shift. The theory of the measurements of the thermal conductivity and hemispherical total emissivity will be explained in Sec. II B.

B. Measurement of thermal conductivity and hemispherical total emissivity from the phase shift

The relation between ϕ and ω as a function of the thermal conductivity and the hemispherical total emissivity is obtainable by solving the following unsteady equation of heat conduction using finite element analysis:[8–10]

$$\rho c_p \frac{\partial T}{\partial t} = \kappa\left[\frac{1}{r^2}\frac{\partial}{\partial r}\left(r^2\frac{\partial T}{\partial r}\right) + \frac{1}{r^2\sin\theta}\frac{\partial}{\partial\theta}\left(\sin\theta\frac{\partial T}{\partial\theta}\right)\right] + Q(r,\theta). \tag{9}$$

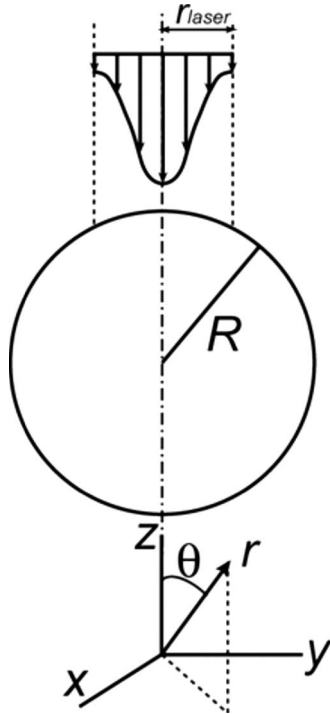In this equation, ρ is the density ($-2 \times 10^{-4}T + 2.9147$

FIG. 2. Schematic diagram of modulated laser calorimetry in spherical coordinates.
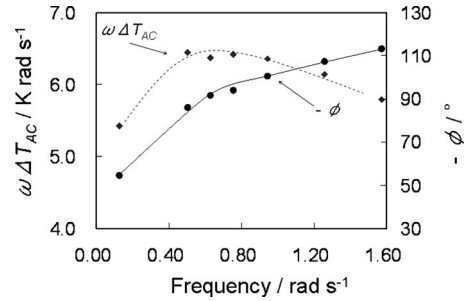

FIG. 3. $\omega\Delta T_{\mathrm{amp}}$ and phase difference ϕ as a function of the modulation angular frequency. The solid line depicts the curve fit for determination of the hemispherical total emissivity and thermal conductivity.

$\times 10^3$ kg m^{-3});[12] c_p represents the isobaric mass heat capacity (1061 ± 184 J kg^{-1} K^{-1}), which was measured for the present study, as shown in the Sec. IV; κ is the thermal conductivity (W m^{-1} K^{-1}); and $Q(r, \theta)$ (W m^{-3}) is the heat generation rate attributable to electromagnetic induction heating. In the spherical coordinate system presented in Fig. 2, $r[m]$ and $\theta[\mathrm{rad}]$, respectively, denote the radial distance and polar angle. The following assumptions are made to apply this unsteady heat conduction equation to our experimental condition: (1) the system is axially symmetric; (2) the thermophysical properties are constant within the temperature variation during the calorimetry measurement; (3) laser power is absorbed on the liquid surface depending on its absorptivity; (4) the distribution of laser intensity is Gaussian; (5) the heat loss from the sample surface is that by radiation alone; and (6) the heat transfer in the liquid silicon is governed by conduction.

Boundary conditions (i) of the laser-irradiated area, (ii) of the non-laser-irradiated area, and (iii) of the centerline of the liquid silicon are given as

$$-\kappa\frac{\partial T}{\partial n} = \sigma\varepsilon(T^4 - T_\infty^4) - \frac{2\alpha P_0}{\pi r_{\mathrm{laser}}^2}\exp\left[-\frac{2R^2\sin^2\theta}{r_{\mathrm{laser}}^2}\right]$$
$$\times(-\boldsymbol{n}\cdot\boldsymbol{e}_{\mathrm{laser}}), \tag{10}$$

and

$$-\kappa\frac{\partial T}{\partial n} = \sigma\varepsilon(T^4 - T_\infty^4), \tag{11}$$

and

$$-\kappa\frac{\partial T}{\partial \theta} = 0, \tag{12}$$

where P_0 (W) is the laser power, R (m) is the radius of the sample, n is the normal unit vector, and r_{laser} (m) and $\boldsymbol{e}_{\mathrm{laser}}$, respectively, denote the radius and unit vector of the laser. Solving the equation of heat conduction (6) with the boundary conditions, the phase shift is expressed as

$$\phi = \tan^{-1}\left(\frac{\mathrm{average}(\Delta T_{\mathrm{ac}}^{\mathrm{out}})}{\mathrm{average}(\Delta T_{\mathrm{ac}}^{\mathrm{in}})}\right), \tag{13}$$

$$\mathrm{average}(\Delta T_{\mathrm{ac}}^{\mathrm{in}}) = \frac{1}{S_{\mathrm{pyrometer}}}\int_S \Delta T_{\mathrm{ac}}^{\mathrm{in}}(r, \theta)r\sin\theta\sqrt{(dr)^2 + (rd\theta)^2}, \tag{14}$$

and

$$\mathrm{average}(\Delta T_{\mathrm{ac}}^{\mathrm{out}}) = \frac{1}{S_{\mathrm{pyrometer}}}\int_S \Delta T_{\mathrm{ac}}^{\mathrm{out}}(r, \theta)r\sin\theta$$
$$\times\sqrt{(dr)^2 + (rd\theta)^2}, \tag{15}$$

where $\Delta T_{\mathrm{ac}}^{\mathrm{in}}$ and $\Delta T_{\mathrm{ac}}^{\mathrm{out}}$, respectively, denote the in phase and out of phase of the temperature amplitude and $S_{\mathrm{pyrometer}}$ is the spot area of the pyrometer.

Figure 3 shows an example of the relation between ϕ and ω. The solid circles represent the experimentally obtained phase shifts from a series of modulation heating; the solid line shows the curve fitted to the numerically obtained ϕ-ω relation[8–10] from experimentally obtained data. The phase shift at lower modulation frequency is controlled predominantly by hemispherical total emissivity. On the other hand, the phase shift at a higher frequency is controlled mainly by thermal conductivity. Consequently, this curve fitting over the entire frequency range can separately determine both thermal conductivity and hemispherical total emissivity.

An example of $\omega\Delta T_{\mathrm{ac}}$, dependence on ω, is also shown as solid diamonds in Fig. 3. The value of $\omega\Delta T_{\mathrm{ac}}$ has a maximum around ω, which gives $\phi=90°$, as predicted by the principle of ac calorimetry. The adiabatic condition was satisfied at this modulation frequency. Therefore, the isobaric molar heat capacity of the sample was determined using this maximum value of $\omega\Delta T_{\mathrm{ac}}$.

C. Measurement of hemispherical total emissivity from the cooling curve

When the isobaric molar heat capacity was determined independently using Eq. (4), the hemispherical total emissivity of the levitated liquid silicon droplet in vacuum can also be determined from the radiative cooling curve. Under the condition of $T_0 \gg \Delta T_{dc}$, the time dependence of the temperature after laser irradiation ceases is expressible as follows:

$$T(t) = T_0 + \Delta T_{dc} \exp(-t/\tau_r). \qquad (16)$$

By fitting the cooling curve to the exponential function presented above, the value of τ_r is determined; consequently, the emissivity can be determined using Eq. (6).

III. EXPERIMENTAL

A single crystalline silicon cube ($7 \times 7 \times 7$ mm³) was placed at the center of the rf coil (15 kW, 200 kHz) in a vacuum chamber. Before the experiment, the chamber was evacuated using a rotary pump in combination with a turbomolecular pump to obtain a vacuum level of 10^{-3} Pa. The silicon was preheated using irradiation of a semiconductor laser up to a temperature at which the electrical resistivity was reduced sufficiently to levitate liquid silicon using the applied electromagnetic force. A superconducting magnet with a 220 mm bore was used to impose a static magnetic field. The strength of the static magnetic field was 0–4 T to suppress convection in the liquid silicon. The initial temperature of the liquid silicon was controlled using the electric power supply to the rf coil. The top surface of the levitated silicon droplet was heated sinusoidally using a laser. A laser apparatus (NBT-S140-mk II; JENOPTIK Laserdiode Japan Co., Ltd., Tokyo, Japan) was equipped with a fiber-coupling-type cw laser diode. The maximum output power was 140 W at a wavelength of 807 ± 3 nm. A calibrated laser power meter (FieldMate; Coherent, Inc., Portland, OR, USA) evaluated the net laser power through the optical system, which consisted of an optical fiber, a corrective lens, and a glass window within an uncertainty of $\pm 2.4\%$. A two-color pyrometer (IR-CAQ2CS; Chino Corp., Tokyo, Japan) was used with the emissivity ratio of two wavelengths (1350 and 900 nm). The relative uncertainty of the pyrometer is $\pm 0.5\%$ of the temperature; the temperature resolution is 1 K. An aperture was placed between the liquid silicon and the two-color pyrometer to block off the incident laser noise to the pyrometer. The laser power was turned off after the succession of the modulated laser calorimetry; then the silicon liquid was cooled by radiation.

The weight of the silicon sample before and after the experiment was measured to determine the isobaric molar heat capacity. The pyrometer was calibrated using the melting point of the liquid silicon during solidification. Both the laser power and temperature data were recorded with a sampling interval of 20 ms. The crystalline silicon grain reflects the flow in the liquid silicon; it was observed using a high-speed charge coupled device camera to evaluate the effect of the static magnetic field on the convective flow.
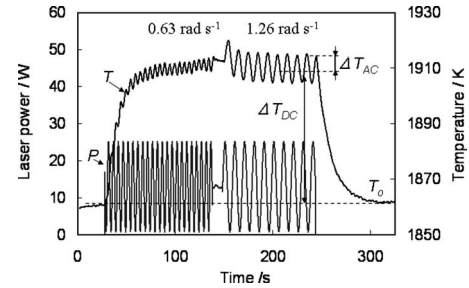

FIG. 4. An example of time dependence of the laser power and the temperature response of liquid silicon during modulated laser calorimetry.

IV. RESULTS

A. Temperature response

Figure 4 shows an example of the temperature response of the noncontact modulated laser calorimetry for the electromagnetically levitated liquid silicon. Initially, the silicon droplet temperature was maintained at T_0 with balancing between the radiative heat loss and rf induction heating. Then the droplet was heated sinusoidally using the laser. The droplet's average temperature gradually increased by ΔT_{dc} from T_0 until the radiative heat loss was balanced with the sum of the rf induction heating and modulated laser heating; subsequently, the temperature reached an ac steady state. A typical example of the temperature response in the ac steady state is shown in Fig. 5 for the modulation frequency of 0.628 rad s⁻¹. The temperature amplitude and the phase shift were measured by changing the modulation angular frequency to obtain both the ϕ-ω and the $\omega \Delta T_{ac}$-ω relation.

Temperature heterogeneity in the sample resulting from modulated laser heating was investigated quantitatively by Tsukada *et al.*[8] In their investigation, the temperature difference between maximum and minimum in the sample was about 13 K because of the high thermal conductivity of liquid silicon. In this experiment, the thermophysical properties of liquid silicon are assumed to be constant during calorimetry measurements within this range of temperature variation.

B. Isobaric molar heat capacity

Figure 6 shows the isobaric molar heat capacity of liquid silicon with data from literature.[13–16] A clear temperature or static magnetic field dependence of the molar heat capacity was not observed. The experimental uncertainty of the molar heat capacity measurements will be discussed in Sec. V A.
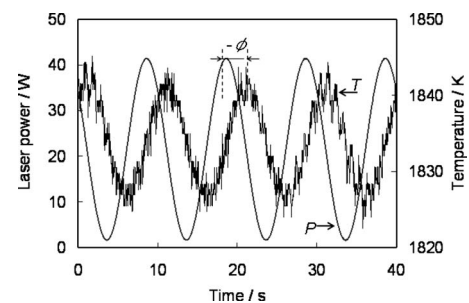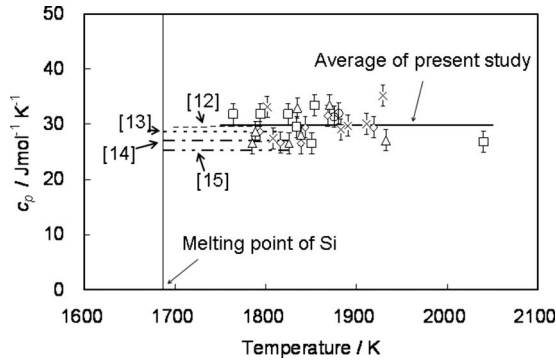

FIG. 5. Temperature response in an ac steady state.

FIG. 6. The isobaric molar heat capacity measured in a static magnetic field at 0.5 T (diamond), 1.0 T (cross), 2.0 (square), 3.0 T (triangle), and 4.0 T (circle) with data from literature. The numbers denote reference numbers. The dotted line indicates the average of our experimental data. The solid line depicts the average of this study.

The average isobaric molar heat capacity of liquid silicon is 30 ± 5 J mol^{-1} K^{-1} at temperatures of 1750–2050 K. The experimental uncertainty presented in the above value is double the standard deviation for all the presented data. The present results show good agreement with the literature data reported by Kantor *et al.*,[13] Yamaguchi and Itagaki,[14] and Olette,[16] which were measured using the drop calorimetry method.

C. Hemispherical total emissivity

The hemispherical total emissivity of liquid silicon determined from the phase shift is shown in Fig. 7. Similarly to the case of the molar heat capacity, neither clear temperature nor static magnetic field dependence of the hemispherical total emissivity was observed. The average hemispherical total emissivity is 0.27 ± 0.03 at temperatures of 1750–1910 K. Recently, the ratio of the hemispherical total emissivity to the molar heat capacity of liquid silicon was measured using the radiative cooling curve of electrostatically levitated liquid silicon.[17] On the other hand, the hemispherical total emissivity and the molar heat capacity were determined independently using modulated laser calorimetry.

The hemispherical total emissivity of the liquid silicon was also obtained from the radiative cooling curve. Figure 8(a) shows the radiative cooling curve of the liquid silicon.
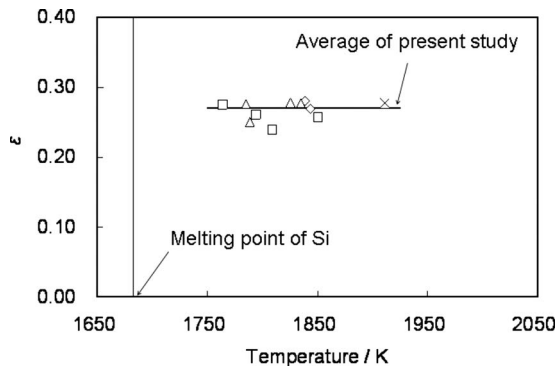

FIG. 7. The hemispherical total emissivity of the liquid silicon obtained from the phase shift measured in a static magnetic field at 0.5 T (diamonds), 1.0 T (crosses), 2.0 T (squares), 3.0 T (triangles), and 4.0 T (circles). The solid line depicts the average obtained in this study.
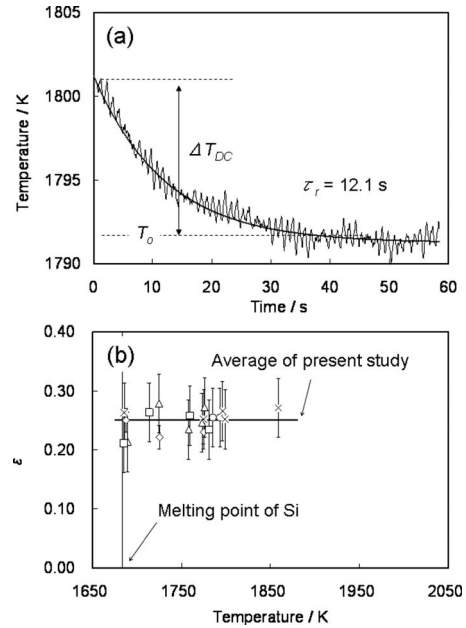

FIG. 8. (a) Change in temperature of silicon droplet after turning off the laser power. (b) The hemispherical total emissivity determined from the radiative cooling curve measured in a static magnetic field at 0.5 T (diamond), 1.0 T (cross), 2.0 (square), 3.0 T (triangle), and 4.0 T (circle). The solid line in (b) depicts the average of this study.

By curve fitting of Eq. (16), the external thermal relaxation time attributable to radiative cooling was 12.1 s. The hemispherical total emissivity of liquid silicon determined from
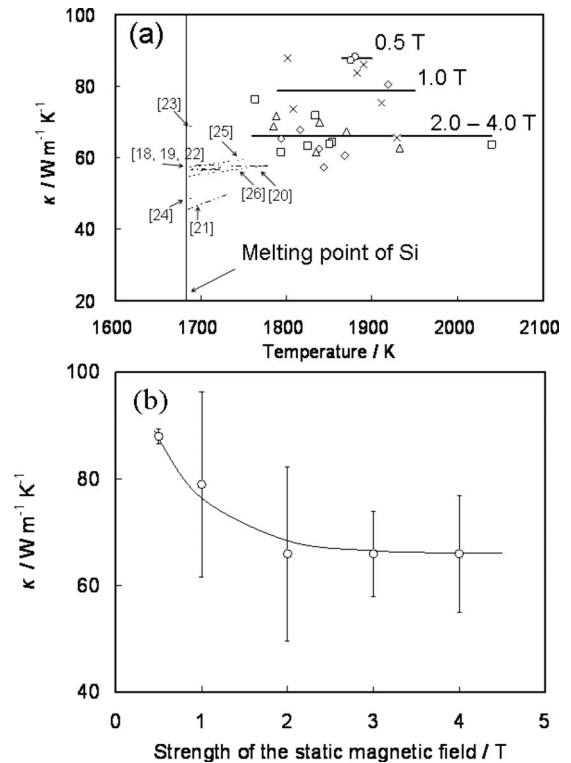

FIG. 9. (a) The thermal conductivity measured in a static magnetic field at 0.5 T (diamonds), 1.0 T (crosses), 2.0 (squares), 3.0 T (triangles), and 4.0 T (circles) together with data from literature. The numbers are reference numbers. The solid lines show the average of our experimental data obtained at respective strengths of the static magnetic field. (b) The apparent thermal conductivity measured at respective strengths of the static magnetic field.
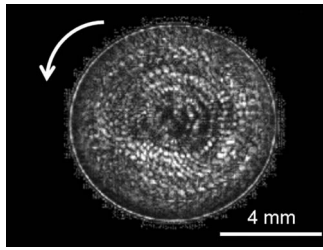
FIG. 10. AQ: PLEASE PROVIDE CAPTION FOR FIGURE 10, SINCE IT IS CITED IN TEXT.

the radiative cooling curve is shown in Fig. 8(b). The average of the hemispherical total emissivity determined from the radiative cooling curve is 0.25 ± 0.04. This result agrees with data obtained from the phase shift (Fig. 7) within experimental uncertainty. Both experimental uncertainties of the hemispherical total emissivity are double of the standard deviation for all present data.

D. Thermal conductivity

Figure 9(a) shows the thermal conductivity of liquid silicon against the temperature, with data from literature.[18–26] Figure 9(b) shows the dependence of the average apparent thermal conductivity on the strength of static magnetic field. The apparent thermal conductivity is 88 W m^{-1} K^{-1} at 0.5 T. However, the apparent thermal conductivity decreases as the strength of the static magnetic field increases. Finally, the value converges on the value of 66 ± 11 W m^{-1} K^{-1} at 2 T or larger. The experimental uncertainty of the thermal conductivity is double the standard deviation for all data greater than 2 T. No marked temperature dependence of thermal conductivity was observed in the experimental temperature region. Our data measured above 2 T are in the high-temperature extended region of the literature thermal conductivities that have been measured[18–22] or calculated using the Wiedemann–Franz law[23–26] [Fig. 9(a)].

Figure 10 shows a top view of the motion of the nucleated silicon grains on levitated liquid silicon at 1 T. The grains are arranged concentrically. This observation also suggests that convection is suppressed in the static magnetic field. The agreement indicates that the convergence at 2 T or larger is attributable to suppression of convection, as discussed in Sec. V C.

V. DISCUSSION

A. Verification of $K_r/K_c \leq 0.01$ in modulation calorimetry

The condition of $K_r/K_c \leq 0.01$ should be satisfied for justification of the modulated laser calorimetry for liquid silicon. However, it is difficult to estimate the volume that is heated directly by laser irradiation (V_h) for quantitative evaluation of K_c. Here, the Biot number relevant to the value of K_r/K_c, defined as

$$\mathrm{Bi} = \frac{4\varepsilon\sigma T_0^3}{\kappa/R}, \tag{17}$$

is used for evaluation. The estimated Bi number is 0.019–0.031 under the present conditions, depending on temperature. This value indicates that the experimental postulate that heat transfer to the external heat bath is much less than the heat transfer to the inner part, i.e., the condition of $K_r/K_c \leq 0.01$ would be fundamentally satisfied.

The correction function f is obtainable from the external and internal thermal relaxation times using Eq. (8). The external relaxation time τ_r is estimated from the cooling curve analysis. Using τ_r and Eq. (5), the internal relaxation time τ_c is evaluated by fitting the frequency dependence of the phase shift in Fig. 3. The values of τ_r and τ_c are 12.1 and 0.16 s, respectively. Consequently, the value of f has a maximum value of 0.99 at frequencies between 0.628 and 0.754 rad s^{-1}.

B. Uncertainty in the molar heat capacity measurements

The uncertainty in the heat capacity depends not only on the correction function but also on the uncertainties of (1) normal spectral emissivity, (2) laser power, (3) modulation frequency, (4) temperature amplitude, and (5) sample mass. The respective contributions of uncertainty factors on the measurement are listed in Table I. The uncertainty in the sample mass results from evaporation during the modulation experiment. Results show that uncertainties in normal spectral emissivity and temperature amplitude are a major contribution. The combined uncertainty on the c_p measurement is expressed using the following:

TABLE I. List of uncertainty factors of the isobaric molar heat capacity measurement. Experimental condition: $T = 1827$ K, $R = 4.1$ mm, $\omega = 0.63$ rad s^{-1}, and $c_p = 26.71$ J mol^{-1} K^{-1}.

Factor	Standard uncertainty	Sensitivity coefficient	Contribution
ε_s	0.223 ± 0.001	$\partial c_p/\partial\varepsilon_s = 121.69$ J mol^{-1} K^{-1}	0.122
P	19.40 ± 0.46 W	$\partial c_p/\partial P = 1.31$ s mol^{-1} K^{-1}	0.61
ω	$0.63 \pm 1.5 \times 10^{-5}$ rad s^{-1}	$\partial c_p/\partial\omega = -40.56$ J rad mol^{-1} K^{-1} s^{-1}	6.44×10^{-4}
ΔT_{ac}	10.14 ± 0.5 K	$\partial c_p/\partial\Delta T_{\mathrm{ac}} = -2.52$ J mol^{-1} K^{-2}	1.26
m	0.701 ± 0.01 g	$\partial c_p/\partial m = -36.46$ J g^{-2} K^{-2}	0.36
Combined uncertainty	$\cdots$	$\cdots$	1.9

TABLE II. List of uncertainty factors for total hemispherical emissivity measurement

Factor	Standard uncertainty	Sensitivity coefficient	Contribution
c_p	29.8 ± 5.2 J mol^{-1} K^{-1}	$\partial \varepsilon / \partial c_p = 0.31$ J^{-1} mol K	0.063
τ_r	12.1 ± 0.1 s	$\partial \varepsilon / \partial \tau_r = -0.02$ s^{-1}	-0.002
T_0	1792 ± 18 K	$\partial \varepsilon / \partial T_o = -4.88 \times 10^{-4}$ K^{-1}	-0.009
m	0.701 ± 0.01 g	$\partial \varepsilon / \partial m = -0.44$ g^{-1}	-0.004
r	$4.03 \pm 10 \times 10^{-5}$ mm	$\partial \varepsilon / \partial r = -0.01$ m^{-1}	-1.00×10^{-7}
Combined uncertainty	$\cdots$	$\cdots$	0.05

$$[\sigma(c_p)]^2 = \left[\left(\frac{\partial c_p}{\partial \varepsilon_s}\right) \times \sigma(\varepsilon_s)\right]^2 + \left[\left(\frac{\partial c_p}{\partial p}\right) \times \sigma(p)\right]^2$$
$$+ \left[\left(\frac{\partial c_p}{\partial \omega}\right) \times \sigma(\omega)\right]^2 + \left[\left(\frac{\partial c_p}{\partial \Delta T_{ac}}\right)\right.$$
$$\left. \times \sigma(\Delta T_{ac})\right]^2 + \left[\left(\frac{\partial c_p}{\partial m}\right) \times \sigma(m)\right]^2. \quad (18)$$

Consequently, the combined uncertainty is evaluated as 1.9 J mol^{-1} K^{-1} in the molar heat capacity of liquid silicon.

C. Uncertainty in the hemispherical total emissivity

The uncertainty in the hemispherical total emissivity measured using the radiative cooling curve depends on the uncertainties of (1) heat capacity, (2) external relaxation time, (3) initial temperature, (4) sample radius, and (5) mass. Consequently, the combined uncertainty of the ε is expressed using the following equation:

$$[\sigma(\varepsilon)]^2 = \left[\left(\frac{\partial \varepsilon}{\partial c_p}\right) \times \sigma(c_p)\right]^2 + \left[\left(\frac{\partial \varepsilon}{\partial \tau_r}\right) \times \sigma(\tau_r)\right]^2$$
$$+ \left[\left(\frac{\partial \varepsilon}{\partial T_0}\right) \times \sigma(T_0)\right]^2 + \left[\left(\frac{\partial \varepsilon}{\partial R}\right) \times \sigma(R)\right]^2$$
$$+ \left[\left(\frac{\partial \varepsilon}{\partial m}\right) \times \sigma(m)\right]^2. \quad (19)$$

The contribution of each uncertainty factor on the measurement of the hemispherical total emissivity is listed in Table II. The uncertainty of the external relaxation time obtained from the fitting curve is 0.1 s. The relative uncertainty of T_0 is 1%. The uncertainty in the sample radius is calculated from the sample mass using the liquid silicon density reported in an earlier study.[12] Consequently, the combined uncertainty in hemispherical total emissivity is ± 0.05.

D. Validity of the thermal conductivity and emissivity of the silicon liquid

The velocity of magnetohydrodynamic convection in the electromagnetically levitated droplet generally reaches $10-40$ cm s^{-1} without a static magnetic field.[27–30] Tsukada *et al.*[31] demonstrated, using numerical analysis, that the maximum flow rate in the electromagnetically levitated liquid silicon is significantly reduced with increasing strength of the static magnetic field. At 4 T of the static magnetic field, the maximum flow velocity near the centerline is reduced to less than 1 cm s^{-1}. The converged thermal conduc-

tivity of liquid silicon in the static magnetic field of greater than 2 T suggests that the convection was suppressed to a sufficiently low level to measure the thermal conductivity. It can be concluded that applying the static magnetic field of 2 T enables accurate measurement of the thermal conductivity of liquid silicon.

Sensitivity analysis of the determination of thermal conductivity of the liquid silicon by fitting the relation between ϕ and ω was carried out by Tsukada *et al.*[8] using a numerical simulation. The sensitivity of the phase shift for thermal conductivity is considerable at higher modulation frequency. The deviation of 4° corresponds to the uncertainty of 10% in the thermal conductivity at the modulation frequency of 1.57 rad s^{-1}.

On the other hand, the sensitivity for hemispherical total emissivity becomes significant at a lower frequency. For precise determination of emissivity, ϕ at $\omega < 0.3$ rad s^{-1} is necessary.[9] In this study, the frequency range is sufficiently wide to determine both thermal conductivity and emissivity experimentally.

VI. CONCLUSION

We measured the thermophysical properties of liquid silicon by conducting levitation calorimetry coupled with the imposition of the static magnetic field for suppression of convection. The results are summarized as follows.

The isobaric molar heat capacity is 30 ± 5 J mol^{-1} K^{-1} (1750–2050 K). The hemispherical total emissivity is 0.27 ± 0.02 (1750–1910 K); the thermal conductivity is 66 ± 11 W m^{-1} K^{-1} (1750–2050 K). The convection in the electromagnetically liquid silicon droplet is suppressed sufficiently to enable measurement of the thermal conductivity in the static magnetic field above 2 T.

[1] T. Hibiya and I. Egry, Meas. Sci. Technol. **16**, 317 (2005).
[2] M. Mito, T. Tsukada, M. Hozawa, C. Yokoyama, Y. R. Li, and N. Imaishi, Meas. Sci. Technol. **16**, 457 (2005).
[3] H.-J. Fecht and W. L. Johnson, Rev. Sci. Instrum. **62**, 1299 (1991).
[4] R. K. Wunderlich and H.-J. Fecht, Appl. Phys. Lett. **62**, 3111 (1993).
[5] R. K. Wunderlich, D. S. Lee, W. K. Johnson, and H.-J. Fecht, Phys. Rev. B **55**, 26 (1997).
[6] R. K. Wunderlich and H.-J. Fecht, Meas. Sci. Technol. **16**, 402 (2005).
[7] H. Yasuda, I. Ohnaka, Y. Ninomiya, R. Ishii, S. Fujita, and K. Kishio, J. Cryst. Growth **260**, 475 (2004).
[8] T. Tsukada, H. Fukuyama, and H. Kobatake, Int. J. Heat Mass Transfer **50**, 3054 (2007).
[9] H. Fukuyama, H. Kobatake, K. Takahashi, I. Minato, T. Tsukada, and S. Awaji, Meas. Sci. Technol. **18**, 2059 (2007).
[10] H. Kobatake, H. Fukuyama, I. Minato, T. Tsukada, and S. Awaji, Appl. Phys. Lett. **90**, 94102 (2007).
[11] H. Kawamura, H. Fukuyama, M. Watanabe, and T. Hibiya, Meas. Sci. Technol. **16**, 386 (2005).
[12] K. Higuchi, K. Kimura, A. Mizuno, M. Watanabe, Y. Katayama, and K. Kuribayashi, Meas. Sci. Technol. **16**, 381 (2005).
[13] P. B. Kantor, A. M. Kisel, and E. N. Fomichev, Ukr. Fiz. Zh. **5**, 358 (1960).
[14] K. Yamaguchi and K. Itagaki, J. Therm Anal. Calorim. **69**, 1059 (2002).
[15] *NIST-JANAF Thermochemical Tables*, 4th ed., edited by M. W. Chase, Jr. (American Institute of Physics, USA, 1998).
[16] M. Olette, Compt. Rend. **244**, 1033 (1957).
[17] W. K. Rhim and K. Ohsaka, J. Cryst. Growth **208**, 313 (2000).
[18] K. Yamamoto, T. Abe, and S. Takasu, Jpn. J. Appl. Phys., Part 1 **30**, 2423 (1991).
[19] E. Takasuka, E. Tokizaki, K. Terashima, and S. Kimura, Proceedings of the Fourth Asian Thermophysical Properties Conference, 1995 (unpublished), Vol. B1d3, p. 89.
[20] T. Nishi, H. Shibata, and H. Ohta, Mater. Trans. **44**, 2369 (2003).
[21] H. Nagai, Y. Nakata, T. Tsurue, H. Minagawa, K. Kamada, E. Gustafsson, and T. Okutani, Jpn. J. Appl. Phys., Part 1 **39**, 1405 (2000).
[22] E. Yamasue, M. Susa, H. Fukuyama, and K. Nagata, J. Cryst. Growth **234**, 121 (2002).
[23] N. E. Cusack, Rep. Prog. Phys. **26**, 361 (1963).
[24] V. M. Glazov, V. B. Kol'tsov, and V. A. Kurbatov, Sov. Phys. Semicond. **20**, 1351 (1986).
[25] H. Sasaki, A. Ikari, K. Terashima, and S. Kimura, Jpn. J. Appl. Phys., Part 1 **34**, 3426 (1995).
[26] H. S. Schnyders and J. B. Van Zytveld, J. Phys.: Condens. Matter **8**, 10875 (1996).
[27] J. H. Zong, B. Li, and J. Szekely, Acta Astronaut. **26**, 435 (1992).
[28] B. Q. Li and S. P. Song, Microgravity Sci. Technol. **11**, 134 (1998).
[29] V. Bojarevics and K. Pericleous, ISIJ Int. **43**, 890 (2003).
[30] R. W. Hyers, Meas. Sci. Technol. **16**, 394 (2005).
[31] T. Tsukada, K. Sugioka, H. Fukuyama, and H. Kobatake (unpublished).